Rare Metal Materials and Engineering
Volume 51, Issue 11, November 2022
Available online at www.rmme.ac.cn

Science Press

Cite this article as: Qiu Yanru, Wang Xianhui, Liang Yan, et al. Preparation and Electrical Characteristics of Novel AgZrB$_2$ Contact Materials[J]. Rare Metal Materials and Engineering, 2022, 51(11): 4031-4038.

ARTICLE

Preparation and Electrical Characteristics of Novel AgZrB$_2$ Contact Materials

Qiu Yanru, Wang Xianhui, Liang Yan, Ni Jingyi, Liu Jituo, Li Hangyu, Chen Qiuyu

School of Materials Science and Engineering, Xi'an University of Technology, Xi'an 710048, China

Abstract: The novel AgZrB$_2$ electrical contact materials with different ZrB$_2$ contents were prepared by the combination method of ultrasonication, ball milling, and spark plasma sintering, and the arc erosion and material transfer behavior were investigated by the electrical contact tests. The results show that the ZrB$_2$ content significantly affects the arc erosion resistance of AgZrB$_2$ electrical contact materials. The Ag-3wt% ZrB$_2$ contact material presents the stable make/break-arc energy and duration, indicating the excellent arc erosion resistance. However, the increased ZrB$_2$ content results in higher make-arc energy and longer make-arc duration with large fluctuations of break arc energy and duration, leading to the severe arc erosion. This result suggests that the excessive ZrB$_2$ is not beneficial to the enhancement of arc erosion resistance. Moreover, it is found that the Ag-3wt% ZrB$_2$ and Ag-5wt% ZrB$_2$ contact materials have the same material transfer mode from anode to cathode, whereas the Ag-7wt% ZrB$_2$ contact material has the opposite transfer mode from cathode to anode.

Key words: Ag-based electrical contact; ZrB$_2$; arc erosion; material transfer

As the core components of relay, circuit breaker, connector, and switchgear, the electrical contacts have been widely used in aerospace, automobile, military, and household applications[1,2]. To ensure the stability and reliability of electrical system during long-term service, the electrical contact materials should have high electrical and thermal conductivity, outstanding arc erosion resistance, low contact resistance, excellent welding resistance, and good mechanical properties[3,4]. Thus, the Ag-based contact materials have been developed, such as AgNi, AgC, AgSnO$_2$, AgCdO, AgWC, AgZnO, and AgCuO[5-11]. Although AgNi alloy has low contact resistance and good stability, its poor welding resistance and inferior arc erosion resistance under high current restrict the application[12,13]. The AgC alloy possesses excellent welding resistance, but it has poor arc erosion resistance[14]. AgCdO contact material displays superior electrical and mechanical properties, whereas it is toxic to the environment and humanity health[15]. AgSnO$_2$ is also a promising candidate for contact material, but its non-conductive characteristic (due to SnO$_2$ ceramic) will produce high contact resistance during long-term service. Besides, the resultant temperature rise has the negative effect on the stability and reliability of electrical system[16,17].

With the demands of miniaturization, higher power, and multifunction of electronic components and apparatus, it is necessary to develop a novel electrical contact material with enhanced performance. As ZrB$_2$ has unique excellent properties, such as high melting point (>3000 °C), low density (6.09 g/cm^3), excellent conductivity and thermal conductivity, high hardness, good chemical stability, good corrosion resistance, and low coefficient of thermal expansion[18-21], it is reckoned as an ideal reinforcement for the contact material. However, the investigations of electrical behavior of AgZrB$_2$ contact material are rarely reported.

In this research, the AgZrB$_2$ electrical contact materials with different contents of ZrB$_2$ were prepared by powder metallurgy. The arc erosion and material transfer behavior of AgZrB$_2$ contact materials were investigated, and their mechanisms were also discussed.

1 Experiment

The raw materials were dendritic Ag powder (99.9% purity,

Received date: November 17, 2021
Foundation item: National Natural Science Foundation of China (51971173)

Corresponding author: Wang Xianhui, Ph. D., Professor, School of Materials Science and Engineering, Xi'an University of Technology, Xi'an 710048, P. R. China, Tel: 0086-29-82312185, E-mail: xhwang693@xaut.edu.cn

average particle size of 50 μm) and ZrB_2 powder (99.9% purity, average particle size of 1 μm), and their morphologies observed by scanning electron microscope (SEM) are shown in Fig.1a and 1b, respectively. Firstly, the Ag powder and ZrB_2 powder were dispersed in anhydrous ethanol by ultrasonic processing, followed by mechanical stirring, and vacuum drying. Subsequently, the dried powders were mixed at 300 r/min for 4 h in KQM-YB/B planetary ball mill. Finally, the mixed powder was sintered at 750 °C under 35 MPa in LABOX-330 spark plasma sintering furnace with vacuum of 0.1 Pa. The heating rate was 30 °C/min. Fig.1c and 1d show SEM morphologies of the milled compound powder. The electrical conductivity of the contact material was measured by the Model 7501 eddy current gauge, and the relative density was determined by the Archimedes method. The hardness test was performed by the DHV-1000Z digital microhardness tester, and the mean value of 10 experiment results was used for analysis.

The sintered bulk materials were sliced into the specimens with diameter of 3.8 mm and length of 8 mm. The electric contact tests were conducted under the resistance load of direct current of 24 V/10 A for 5000 operations on the JF04D electric contact test system. The electrode gap, contact force, and switching on-off frequency were 1.5 mm, 0.4 N, and 1 Hz, respectively. The arc duration and arc energy were automatically collected by the electric contact system. The three-dimensional (3D) and two-dimensional (2D) profiles were measured by LEXT OLS4000 laser scanning confocal microscope. The eroded morphologies were observed by the JSM-6700F SEM coupled with energy dispersive spectroscope (EDS). The chemical composition of the eroded surfaces was examined via the XRD-7000 X-ray diffractometer (XRD) and the ESCALAB 250Xi X-ray photoelectron spectroscopy (XPS). The mass change of the contact materials after the electrical contact tests was determined by the FA1104J electronic balance.

2 Results and Discussion

2.1 Microstructure characterization

Fig. 2 displays SEM microstructures of $AgZrB_2$ contact materials with different ZrB_2 contents. The gray area is the Ag matrix, while the black area is ZrB_2. Obviously, a large deformation occurs on the Ag particles after milling. Some ZrB_2 particles are distributed around the deformed silver phase, and other ZrB_2 particles are embedded in the Ag matrix. Additionally, it is also observed from Fig. 2b and 2c that ZrB_2 particles tend to agglomerate when the ZrB_2 content exceeds 5wt%. Fig.2d and 2e show EDS Ag and Zr element distributions of $AgZrB_2$ contact materials with 5wt% ZrB_2. EDS analysis result of the point M marked in Fig.2c is shown in Fig.2f.

2.2 Properties of bulk $AgZrB_2$ contact materials

The relative density, electrical conductivity, and hardness of the bulk $AgZrB_2$ contact materials are shown in Table 1. It can be seen that the high ZrB_2 content results in higher hardness value, but the relative density and electrical conductivity of the $AgZrB_2$ contact material decrease with increasing the ZrB_2 content. Since the pores tend to form in the reinforcement clusters, ZrB_2 with higher content is much easier to agglomerate and thus reduces the relative density. Moreover, the pores existing among ZrB_2 particles also cause the obstacle to electron transport, thereby resulting in the decreased electrical conductivity. The improvement of microhardness can be attributed to the introduction of ZrB_2, which blocks the dislocation movement.

2.3 Arc energy and duration

The arc erosion resistance of $AgZrB_2$ materials is evaluated through the arc energy and duration, as shown in Fig. 3.

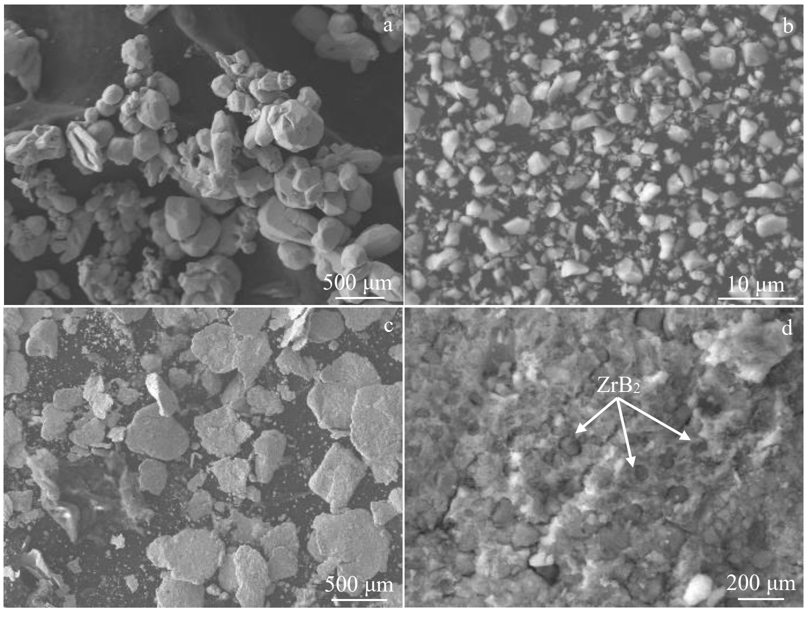

Fig.1 SEM morphologies of raw Ag powder (a), raw ZrB_2 powder (b), and milled compound powder (c, d)

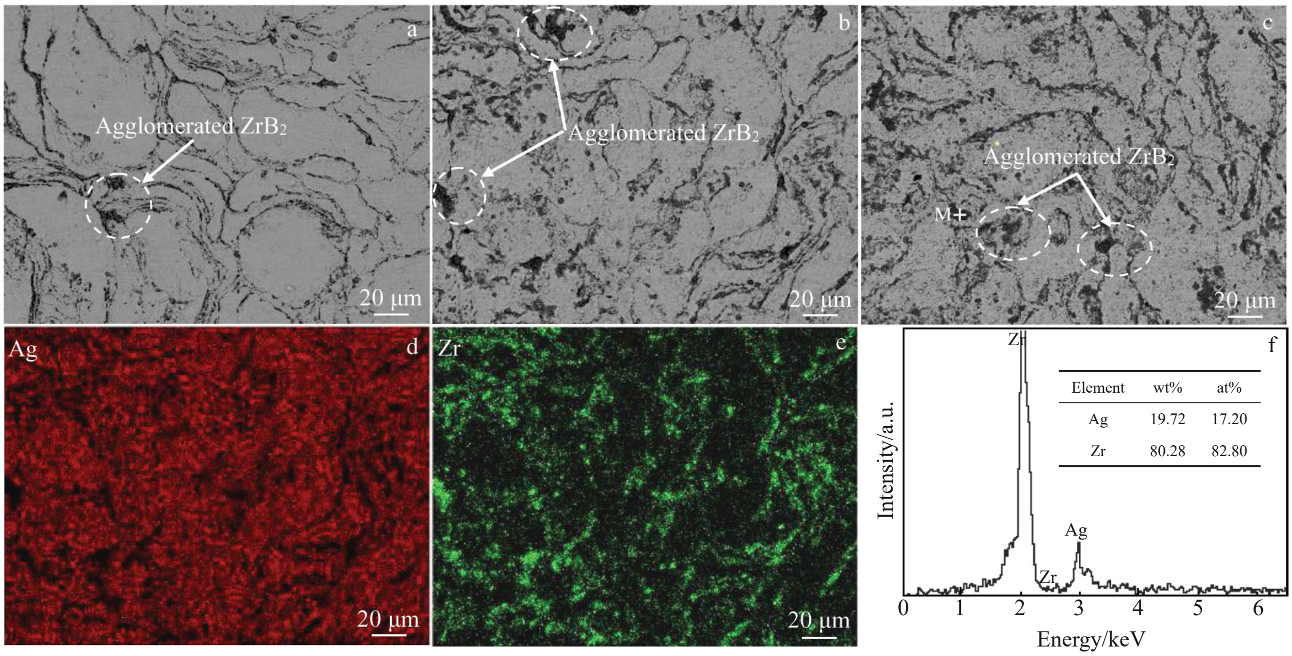

Element	wt%	at%
Ag	19.72	17.20
Zr	80.28	82.80

Fig.2 SEM microstructures of AgZrB$_2$ contact materials with 3wt% ZrB$_2$ (a), 5wt% ZrB$_2$ (b), and 7wt% ZrB$_2$ (c); EDS element distributions of Ag (d) and Zr (e) in AgZrB$_2$ contact materials with 5wt% ZrB$_2$; EDS analysis result of point M marked in Fig.2c (f)

Table 1 Relative density, electrical conductivity, and hardness of different AgZrB$_2$ contact materials

ZrB$_2$ content/ wt%	Relative density/%	Electrical conductivity/%IACS	Hardness, HV/MPa
3	98.9±0.1	90.8±0.3	599.7±9.8
5	96.2±0.1	85.5±1.5	669.3±13.7
7	95.7±0.1	75.8±1.7	690.9±15.7

According to Fig.3a and 3b, the Ag-3wt% ZrB$_2$ and Ag-5wt% ZrB$_2$ contact materials present good stability in the make-arc energy and duration with increasing the operation times. The Ag-3wt% ZrB$_2$ contact material has the low average arc energy and short arc duration, which are 0.53~1.10 J and 9.18~18.75 ms, respectively. Nevertheless, the Ag-5wt% ZrB$_2$ contact material has the average arc energy of 3.56~4.90 J and the average arc duration of 36.97~50.39 ms, which are much larger those of the Ag-3wt% ZrB$_2$ and Ag-7wt% ZrB$_2$ contact materials. For the Ag-7wt% ZrB$_2$ contact material, the make-arc energy and duration are 1.02~2.78 J and 18.40~47.87 ms, respectively, which are obviously lower than those of the Ag-5wt% ZrB$_2$ contact material but higher than those of the Ag-3wt% ZrB$_2$ contact material. In addition, the make-arc energy and duration of all AgZrB$_2$ contact materials have small fluctuations.

Fig. 3c and 3d show the change of break-arc energy and break-arc duration with increasing the operation times, respectively. Evidently, the Ag-3wt% ZrB$_2$ contact material displays better break-arc stability, and the average break-arc energy and duration are 0.10~0.16 J and 1.80~3.00 ms, respectively. However, for the Ag-5wt% ZrB$_2$ and Ag-7wt% ZrB$_2$ contact materials, the break-arc energy and duration have large fluctuations during operation. The break-arc energy and duration of Ag-5wt% ZrB$_2$ contact material are 0.01~0.25 J and 0.07~2.88 ms, respectively; while the break-arc energy and duration of Ag-7wt% ZrB$_2$ contact material are 0.02~0.17 J and 0.42~3.43 ms, respectively.

2.4 Morphologies and chemical composition of arc-eroded electrodes

Fig.4 shows 3D and 2D profiles of the eroded anodes and cathodes after 5000 operation times. According to Fig.4a and 4b, a small number of shallow corrosion pits occur on the anode surface of Ag-3wt% ZrB$_2$ contact material. Some small protrusions appear at the cathode center and the slight erosion occurs at the cathode edge, as shown in Fig. 4c and 4d. According to Fig.4e and 4f, it is found that the anode of Ag-5wt% ZrB$_2$ contact material has serious arc erosion and the contact surface is seriously deformed. Some large corrosion pits appear at the edge of the cathode surface, as shown in Fig. 4g and 4h. Compared with Ag-5wt% ZrB$_2$ contact material, the electrode surface of Ag-7wt% ZrB$_2$ contact material is slightly eroded, as shown in Fig.4i~4l. Among the three contact materials, the most severe erosion occurs in the Ag-5wt% ZrB$_2$ contact material, followed by the Ag-7wt% ZrB$_2$ contact material. The Ag-3wt% ZrB$_2$ contact material has the slightest erosion due to the low arc energy. The higher the arc energy, the more serious the arc erosion.

Fig.5 shows the eroded morphologies of the contact surface of different AgZrB$_2$ contact materials after 5000 times of operation. Apparently, the erosion surface of Ag-3wt% ZrB$_2$ contact material is relatively flat and smooth, as shown in Fig.5a. However, for the Ag-5wt% ZrB$_2$ and Ag-7wt% ZrB$_2$ contact materials, there are a large number of solidified silver traces in the erosion area, suggesting the rough and serious

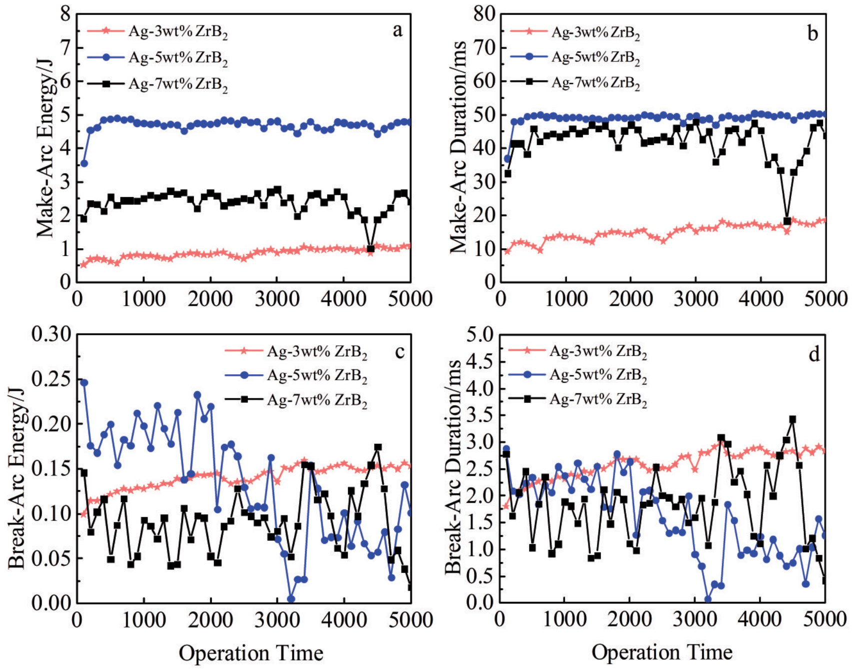

Fig.3 Relationships of make-arc energy (a), make-arc duration (b), break-arc energy (c), and break-arc duration (d) with operation time for AgZrB$_2$ contact materials with different ZrB$_2$ contents

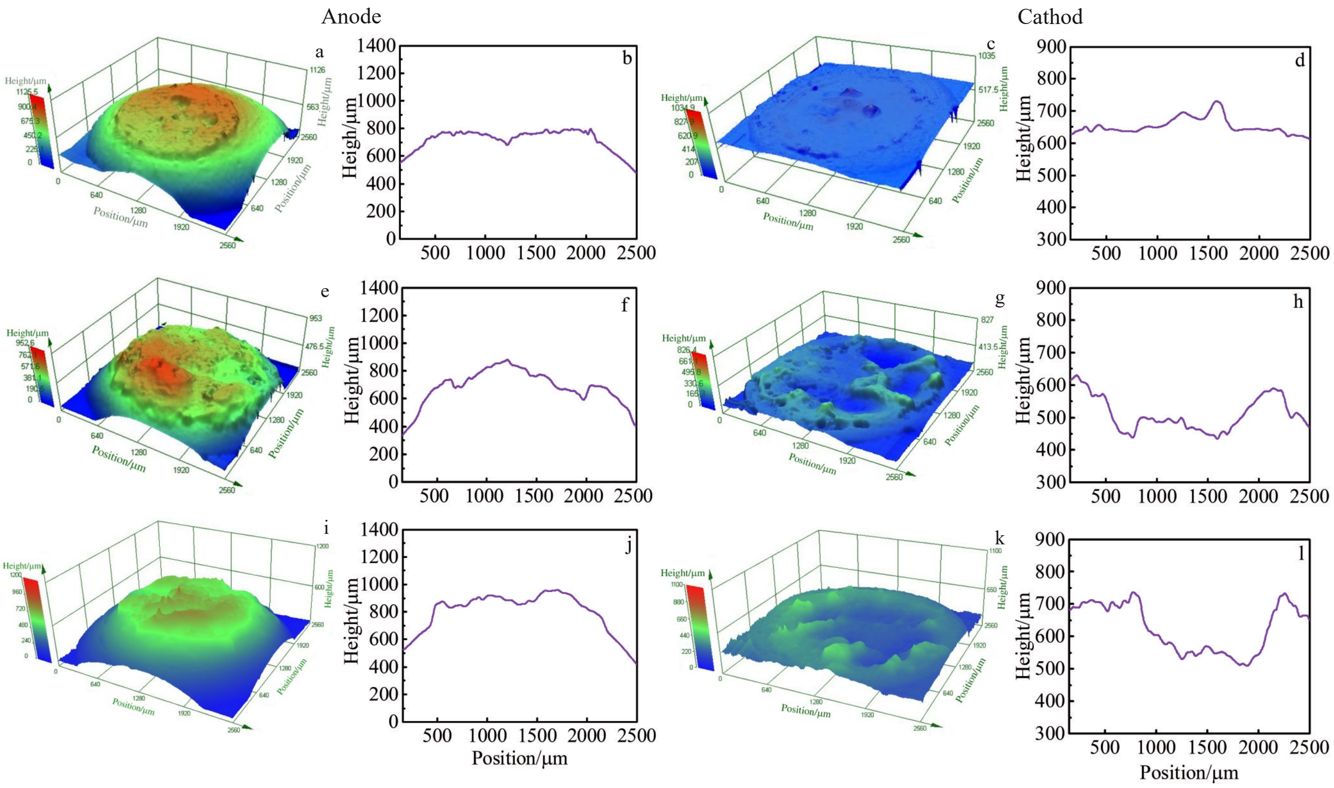

Fig.4 3D and 2D profiles of anodes and cathodes of different AgZrB$_2$ contact materials after 5000 times of operation: (a~d) Ag-3wt% ZrB$_2$, (e~h) Ag-5wt% ZrB$_2$, and (i~l) Ag-7wt% ZrB$_2$

erosion. Fig. 5d shows EDS Ag, Zr, and O element distributions of the eroded surface of Ag-5wt% ZrB$_2$ contact material corresponding to Fig.5b. It is visible that a small amount of O element exists in the eroded surface around Ag and Zr.

XRD pattern of the eroded surface of Ag-7wt% ZrB$_2$ contact material is shown in Fig. 6a. It is obvious that the contact surface is composed of Ag, ZrB$_2$, and ZrO$_2$ phases, indicating that partial ZrB$_2$ is oxidized into ZrO$_2$ during the electrical contact tests. It should be noted that B$_2$O$_3$ cannot be detected, which is mainly due to its low boiling point (1860~

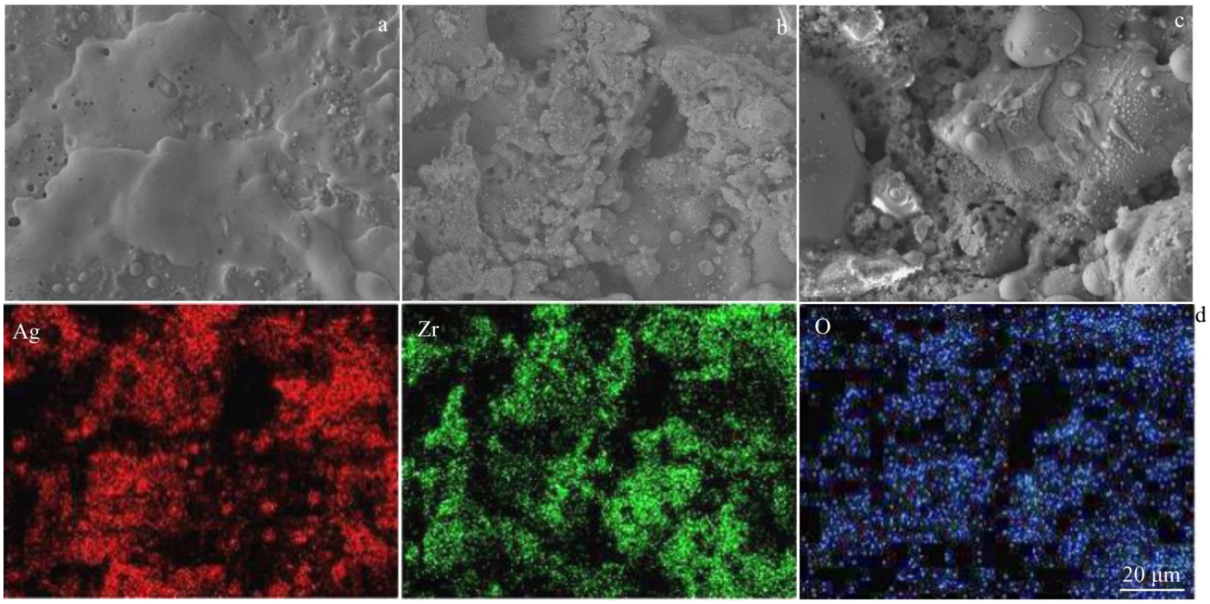

Fig.5 Erosion surface morphologies of Ag-3wt% ZrB_2 (a), Ag-5wt% ZrB_2 (b), and Ag-7wt% ZrB_2 (c) contact materials after 5000 times of operation; corresponding EDS element distributions in Ag-5wt% ZrB_2 contact material (d)

2250 °C), compared with the arc temperature. Because of the high temperature, B_2O_3 generated by the reaction vaporizes and escapes from the electrode surface[22,23], thus resulting in a few residues of B_2O_3 on the electrode surface. XPS analysis was also conducted. As shown in Fig.6b~6e, the peaks of Ag 3d at 368.1 and 374.15 eV confirm the zero valent state of Ag. The two peaks of Zr 3d (Zr $3d_{3/2}$ at 183.2 eV and Zr $3d_{5/2}$ at 185.4 eV) correspond to ZrO_2, and the peak of B 1s at 192.4 eV corresponds to B_2O_3[24]. It is found that the correlation peak of B_2O_3 is much weaker than that of ZrO_2, which is related to the gasification of B_2O_3 under high temperature arc. In addition, the O 1s spectrum is composed of two peaks, and the O 1s peak at 533.0 eV can be attributed to the oxygen in B_2O_3 lattice[25]. Therefore, it can be confirmed that the B_2O_3 is generated during the electrical contact tests.

As an ultra-high temperature conductive ceramic, the ZrB_2 has high melting point and excellent electrical and thermal conductivity. Due to the good thermal conductivity of ZrB_2, the energy can easily be transferred from the contact surface and the surface temperature is reduced during the electrical contact tests[26,27]. Once the temperature is above 800 °C, partial ZrB_2 is oxidized progressively into ZrO_2 and B_2O_3, which can be expressed by Eq.(1) [28,29], as follows:

$$2ZrB_2+5O_2\,(g)\rightarrow 2ZrO_2+2B_2O_3 \qquad (1)$$

The Gibbs free energy of the reaction in Eq.(1) is shown in Fig. 6f. These oxidation products affect the arc erosion resistance of $AgZrB_2$ contact materials. Due to the low thermal conductivity of ZrO_2[30], the formation of ZrO_2 reduces the heat transfer and oxygen diffusion towards the underlying material, thereby hindering the further oxidation reaction[31,32]. Besides, the evaporation and heat absorption of B_2O_3 can also effectively reduce the temperature of electrode surface[31]. Thus, the combined effects reduce the volatilization of molten silver and the content of charged particles in the electrode gap, promoting the rapid extinction of arc. Hence, the Ag-3wt% ZrB_2 contact material has the low and stable arc energy and duration with superior electrical characteristics.

With increasing the ZrB_2 content, the non-conductive oxides, such as ZrO_2 and B_2O_3 ceramics, are further increased on the contact surface. ZrO_2 has little impact on the arc, because the O_2 generated by ZrO_2 decomposition under the arc action acts as the role of arc extinguishing. Zr ions are oxidized or dissolved in the Ag molten pool again during the cooling process, and the surface content reaches the dynamic equilibrium under the action of multiple arcs. As for the B_2O_3 products, partial B_2O_3 is evaporated and dissipated, while the rest B_2O_3 decomposes to form B and O_2. Then, the B is oxidized again to generate B_2O_3. These non-conductive B_2O_3 and B with very low density (B_2O_3: 2.46 g/cm^3; B: 2.34 g/cm^3) are easy to aggregate on the eroded surface, resulting in the increased contact resistance, rapid temperature rise, and reduced arc stability. Therefore, the Ag-5wt% ZrB_2 contact material with higher arc energy and longer duration has more severe arc erosion. For Ag-7wt% ZrB_2 contact material, the formation of more B_2O_3 products causes the change of the contact surface properties, resulting in the unstable arc. Meanwhile, due to the densification and continuity of the oxide film, it is difficult for the silver to melt or vaporize, thereby reducing the concentration of metal ions in the pole gap, causing the difficulty in maintenance of the normal arc combustion, and even destroying the normal conduction of electrical contacts. As a result, the Ag-7wt% ZrB_2 contact material with relatively lower arc energy and shorter duration presents less arc erosion, compared with the Ag-5wt% ZrB_2 contact material.

2.5 Material transfer

Fig. 7 shows the mass changes of different contact pairs after 5000 times of operation. Generally, the material transfer

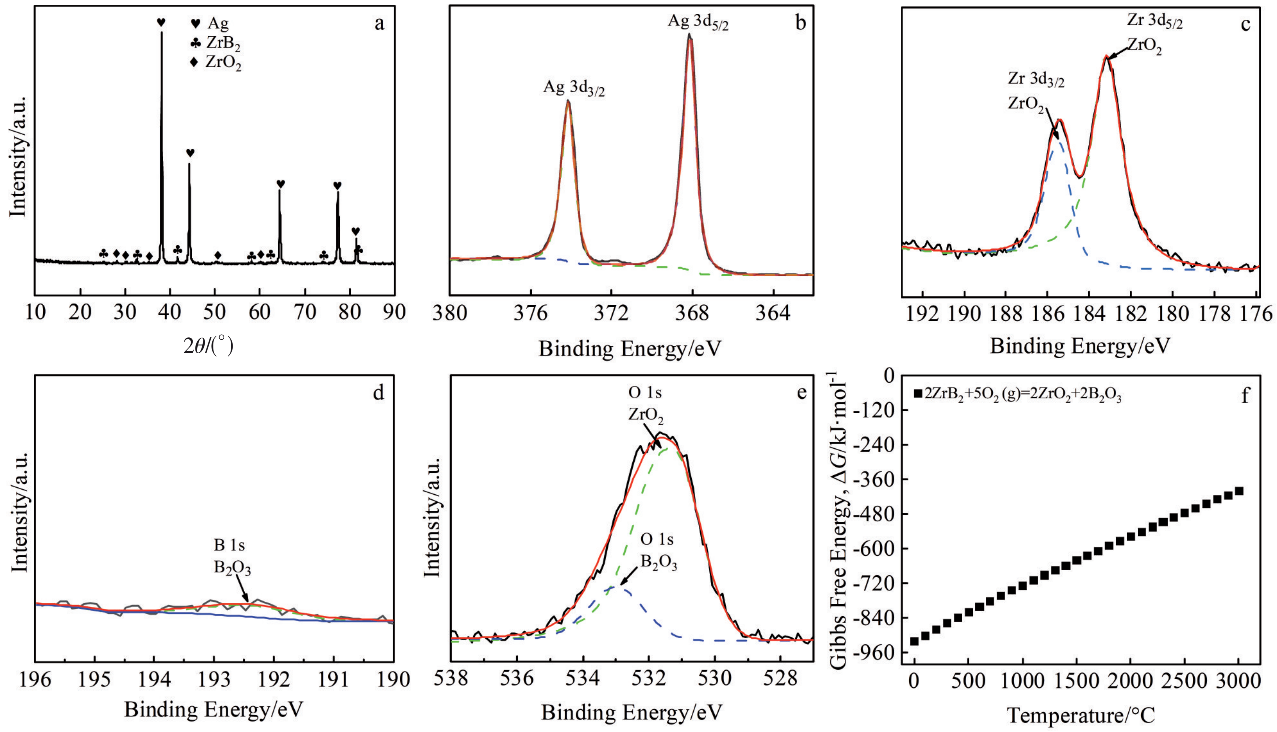

Fig.6 XRD pattern of eroded surface of Ag-7wt% ZrB_2 contact material (a); XPS spectra of Ag 3d (b), Zr 3d (c), B 1s (d), and O 1s (e) of Ag-7wt% ZrB_2 contact material; Gibbs free energy curve of ZrB_2 oxidation reaction (f)

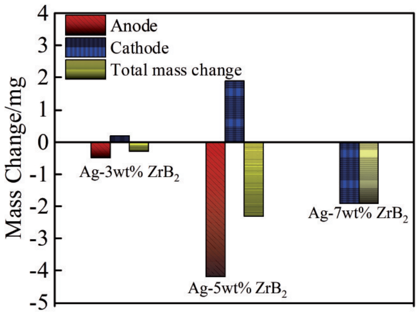

Fig.7 Mass changes of different contact pairs

mode can be well reflected by the mass change. For the Ag-3wt% ZrB_2 contact material, the anode mass loss is 0.5 mg, the cathode mass gain is 0.2 mg, and the total mass change is −0.3 mg. For the Ag-5wt% ZrB_2 contact material, the anode mass loss is 4.2 mg, the cathode mass gain is 1.9 mg, and the total mass change is −2.3 mg. These results display that the material transfer occurs from anode to cathode for these two contact materials. For the Ag-7wt% ZrB_2 contact material, the anode mass does not change, which is mainly due to the balance between the volatilization of partial anode and the partial material transference from the cathode. However, the cathode mass loss is 1.9 mg. Thus, the total mass change is −1.9 mg. This result reveals that the transfer mode of contact material changes as the material transference from cathode to anode.

The change of material transfer mode can be explained by the following reasons. According to the splash and deposition model of micro-particles[33], the metallic phase arc and gaseous phase arc are in the dominant state. For the metallic phase arc, the electrons are emitted from the cathode and gain energy under the action of thermal and electric fields, which can accelerate the material transfer to the anode. The metal vapor is bombarded by electrons to generate metallic ions which are deposited on the cathode under the action of electric field, thus causing the material transfer from the anode to cathode. For the gas phase arc, the gas ions play a dominant role in the electrode gap. The cathode is bombarded by gas ions, and the sputtered particles have sufficient energy to transfer from cathode to anode and then are deposited on the anode. Therefore, the materials transfer from cathode to anode. Since the melting point of Ag (961.8 °C) is far below that of ZrB_2 (3040 °C), Ag is preferentially melted during the electrical contact process, thus leading to the formation of molten Ag pool on the contact surface. In addition, because Ag is easier to evaporate than ZrB_2, a large amount of Ag is ionized into Ag^+/Ag^{2+} ions which surge into the electrode gap. Due to the small electrode gap, the metal ions have the higher concentrations than the gas ions (N^+, N^{2+}, O^{2+}, O^+) between electrodes do. Therefore, the metallic phase arc plays a dominate role during the arc discharge. As a result, the transfer mode of Ag-3wt% ZrB_2 and Ag-5wt% ZrB_2 contact materials is the transference from anode to cathode, as shown in Fig.8a.

For the Ag-7wt% ZrB_2 contact material, the content of oxide film increases on the contact surface, which reduces the Ag volatilization and causes the low concentration of Ag ions in the electrode gap. When the electrode pairs are separated, fewer and fewer particles can maintain the stable combustion of the arc. Therefore, the ionized gas ions of atmosphere

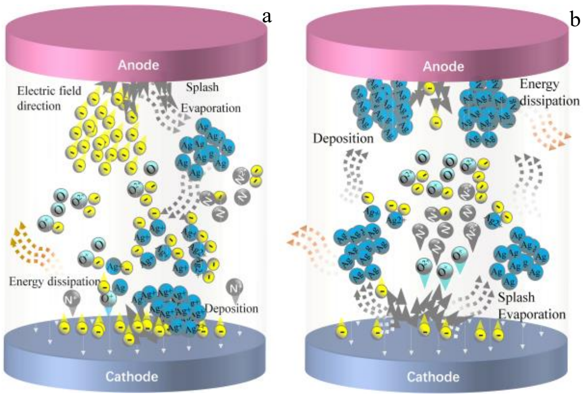

Fig.8 Schematic diagrams of particle transference in metallic phase arc (a) and gaseous phase arc (b)

become the dominant medium between anode and cathode. These gaseous cations are accelerated under the action of electric field and bombard the cathode, causing the cathode particles to splash and to be deposited on the anode. Therefore, the transfer mode of Ag-7wt% ZrB_2 contact material is the material transference from cathode to anode, as shown in Fig.8b.

3 Conclusions

1) The Ag-3wt% ZrB_2 contact material has stable and low arc energy and short arc duration, indicating the excellent arc erosion resistance. This is attributed to the combined action of ZrB_2 and the trace formation of ZrO_2 and B_2O_3 by-products.

2) The increased ZrB_2 content causes the formation of more B_2O_3 products, which results in the increased contact resistance, rapid temperature rise, and serious arc erosion. Moreover, the aggregation of excessive B_2O_3 products influences the electrical conductivity of the contact materials.

3) The appropriate addition of ZrB_2 is beneficial for the enhancement on the arc erosion resistance of Ag-based contact materials.

4) The material transfer mode of Ag-3wt% ZrB_2 and Ag-5wt% ZrB_2 contact materials is from anode to cathode, whereas the Ag-7wt% ZrB_2 contact material has an opposite transfer mode.

References

1 Li Guijing, Yang Tianyang, Ma Yuanyuan *et al*. *Ceramics International*[J], 2020, 46(4): 4897

2 Li Guijing, Ma Yuanyuan, Zhang Xiaolong *et al*. *Ceramics International*[J], 2021, 543(15): 148 812

3 Yang Rui, Liu Shaohong, Chen Jialin *et al*. *Ceramics International*[J], 2018, 45(2): 1881

4 Pietrzak K, Frydman K, Wojcik-Grzybek D *et al*. *Materials Science*[J], 2018, 24(1): 69

5 Wu Chunping, Yi Danqing, Weng Wei *et al*. *Materials and Design*[J], 2015, 85: 511

6 Jiang Peng, Li Feng, Wang Yaping *et al*. *IEEE Transactions on Components and Packaging Technologies*[J], 2006, 29(2): 420

7 Wang Zhe, Wang Yaping. *Journal of Alloys and Compounds*[J], 2019, 774: 1046

8 Morin L, Jeman N B, Jeannot D *et al*. *Proceedings of the Forty-Fifth IEEE Holm Conference on Electrical Contacts*[C]. Pittsburgh: IEEE, 1999: 9

9 Findik F, Uzun H. *Materials and Design*[J], 2003, 24(7): 489

10 Wei Zhijun, Zhang Lingjie, Shen Tao *et al*. *Journal of Materials Engineering and Performance*[J], 2016, 25(9): 3662

11 Wang Zhe, Zhang Xueshuo, Jiang Song *et al*. *Journal of Alloys and Compounds*[J], 2020, 828: 154 412

12 Swingler J. *IET Science, Measurement and Technology*[J], 2011, 5(2): 37

13 Lin Zhijie, Liu Shaohong, Li Jiguang. *Materials and Design*[J], 2016, 108: 640

14 Wingert P C, Allen S E, Bevington R C. *IEEE Transactions on Components, Hybrids, and Manufacturing Technology*[J], 1992, 15(2): 154

15 Wojtasik K, Missol W. *Metal Powder Report*[J], 2004, 57(7): 34

16 Wang Jun, Zhao Haidong, Wang Junbo *et al*. *Journal of Alloys and Compounds*[J], 2019, 770: 920

17 Liu Songtao, Sun Qiaoyan, Wang Junbo *et al*. *Journal of Alloys and Compounds*[J], 2019, 792: 1248

18 Walkosz W, Manandharc K, Trenaryc M *et al*. *Chemical Physics Letters*[J], 2020, 739: 136 984

19 Asl M S, Nayebi B, Ahmadi Z *et al*. *Ceramics International*[J], 2018, 44(7): 7334

20 Vafa N P, Nayebi B, Asl M S *et al*. *Ceramics International*[J], 2016, 42(2): 2724

21 Zhang Y N, Lunghi A, Sanvito S. *Acta Materialia*[J], 2020, 186: 467

22 Zhang S C, Hilmas G E, Fahrenholtz W G *et al*. *Journal of the American Ceramic Society*[J], 2007, 90(11): 3660

23 Rezaie A, Fahrenholtz W G, Hilmas G E. *Journal of the European Ceramic Society*[J], 2007, 27(6): 2495

24 Zhang Zhiguo, Sheng Yinying, Xu Xiwei *et al*. *Advanced Engineering Materials*[J], 2015, 17(9): 1338

25 Lee S H, Sakka Y, Kagawa Y. *Journal of the American Ceramic Society*[J], 2008, 91(5): 1715

26 Li Hangyu, Wang Xianhui, Guo Xiuhua *et al*. *Materials and Design*[J], 2017, 114: 139

27 Ma Q, Tran Q, Tsung-Kuan A *et al*. *MOEMS-MEMS 2007 Micro and Nanofabrication*[C]. San Jose: SPIE, 2007, 6463: 42

28 Tripp W C, Graham H C. *Journal of the Electrochemical Society* [J], 1971, 118(7): 1195

29 Monteverdez F, Bellosi A. *Journal of the Electrochemical Society* [J], 2003, 150(11): B552

30 Li Cuiyan, Li Kezhi, Ouyang Haibo *et al*. *Corrosion Science*[J], 2016, 102: 405

31 Li Xiutao, Shi Jingli, Zhang Guobing *et al*. *Materials Letters*[J], 2006, 60(7): 892

32 Amirsardari Z, Mehdinavaz-Aghdam R, Salavati-Niasari M. *Journal of Materials Science and Technology*[J], 2016, 32(7): 611

33 Chen Z K, Sawa K. *Journal of Applied Physics*[J], 1994, 76(6): 3326

新型$AgZrB_2$触头材料的制备及电气性能

邱艳茹，王献辉，梁　燕，倪菁艺，刘继拓，李航宇，陈秋羽

(西安理工大学 材料科学与工程学院，陕西 西安 710048)

摘　要：采用超声、球磨和放电等离子烧结相结合的方法制备了不同ZrB_2含量（3%，5%，7%，质量分数）的新型$AgZrB_2$触头材料，并通过电接触试验研究了触头材料的电弧侵蚀和材料转移行为。结果表明，ZrB_2含量显著影响$AgZrB_2$触头材料的耐电弧侵蚀性能。Ag-3% ZrB_2触头材料具有稳定的闭合/分断燃弧能量和持续时间，表现出较好的耐电弧侵蚀性能。但是，过多的ZrB_2会导致更高的闭合燃弧能量和更长的闭合燃弧时间，并且分断燃弧能量和时间会产生较大的波动，电弧侵蚀较为严重，这说明过量的ZrB_2不利于提高触头材料的耐电弧侵蚀性能。此外，Ag-3% ZrB_2和Ag-5% ZrB_2触头材料具有相同的材料转移模式——从阳极向阴极转移，而Ag-7% ZrB_2触头材料则呈现出相反的转移模式——从阴极向阳极转移。

关键词：银基电触头；ZrB_2；电弧侵蚀；材料转移

作者简介：邱艳茹，女，1990年生，博士生，西安理工大学材料科学与工程学院，陕西 西安 710048，E-mail：qyrxa_2021@126.com